lubricants

MDPI

Review

Electrical Bearing Damage, A Problem in the Nano- and Macro-Range

Volker Schneider [1,*], Cara Behrendt [2], Pauline Höltje [2], Daniel Cornel [3], Florian Michael Becker-Dombrowsky [4], Steffen Puchtler [4], Francisco Gutiérrez Guzmán [3], Bernd Ponick [2], Georg Jacobs [3] and Eckhard Kirchner [4]

1 Institute of Machine Design and Tribology, Leibniz University Hannover, An der Universität 1, 30823 Garbsen, Germany
2 Institute for Drive Systems and Power Electronics, Leibniz University Hannover, Welfengarten 1, 30167 Hannover, Germany
3 Institute for Machine Elements and Systems Engineering, RWTH Aachen University, Schinkelstrasse 10, 52062 Aachen, Germany
4 Institute for Product Development and Machine Elements, Technical University of Darmstadt, Otto-Berndt-Straße 2, 64287 Darmstadt, Germany
* Correspondence: schneider@imkt.uni-hannover.de; Tel.: +49-511-762-2245

Abstract: Rolling bearings face different damaging effects: Besides mechanical effects, current-induced bearing damage occurs in electrical drive systems. Therefore, it is of increasing interest to understand the differences leading to known electrical damage patterns. It is of utmost importance not to consider the harmful current passage in the machine element as an isolated phenomenon but to take into account the whole drive system consisting of the machine elements, the electric motor and the connected power electronics. This publication works toward providing an overview of the state-of-the-art of research regarding electrical bearing currents.

Keywords: electrical drive system; rolling bearing; electrical bearing damage; bearing current prediction; condition monitoring

Citation: Schneider, V.; Behrendt, C.; Höltje, P.; Cornel, D.; Becker-Dombrowsky, F.M.; Puchtler, S.; Gutiérrez Guzmán, F.; Ponick, B.; Jacobs, G.; Kirchner, E. Electrical Bearing Damage, A Problem in the Nano- and Macro-Range. *Lubricants* **2022**, *10*, 194. https://doi.org/10.3390/lubricants10080194

Received: 4 July 2022
Accepted: 5 August 2022
Published: 21 August 2022

1. Introduction

The damaging effects of electric currents on rolling bearings are described in numerous scientific papers dating back to the mid-20th century when rolling bearings failed in tramway applications [1–3]. With the recent push towards electromobility and the more frequent use of inverter-fed drive systems, the problem of damaging currents gained increasing importance in rolling bearing application and research [4–11]. However, to plan appropriate measures for the design, the question of the electrical behavior of the overall system arises, which may lead to complex approaches [12,13].

The measurement and the analytical description of the electrical stress within inverter-fed drive systems have been subjects of research in the past. These investigations expose the necessity for an analytical calculation approach for the modeling and design of the entire system, including the electrical stresses of all machine elements affected.

This initial publication works towards this need by providing an overview of the state-of-the-art. Therefore, this introduction is followed by an overview of current-related damage based on rolling bearings. In addition, a first literature-based overview attempts to assign typical electrical stress to these damage patterns. The origin of electrical stresses and their corresponding calculation approaches are presented in more detail in Section 2. Section 3 deals with the existing possibilities for describing the electrical behavior of the system, focusing on the electrical machine itself and the rolling bearings installed in the gearbox. In a simplified manner, the electrical behavior of a machine element can be described by its capacitance, resistance, or rather its impedance within the load-carrying and unloaded contacts. Depending on the lubricating conditions, the electrical

behavior is either determined by the machine element properties (dry contact), the lubricant properties (hydrodynamic separation), or by both (mixed friction) as shown in Figure 1. It is important to capture not only the area of hydrodynamic lubrication conditions with an insulating lubricant film but also mixed and dry friction modes as shown in Figure 1 with the increasing likelihood of metallic contact. Finally, possibilities for the measurement of electrical stress or damages in the system, e.g., via contact capacitance measurements, are explained in Section 4. Section 5 summarizes the current state-of-the-art and expresses the needs for future work.

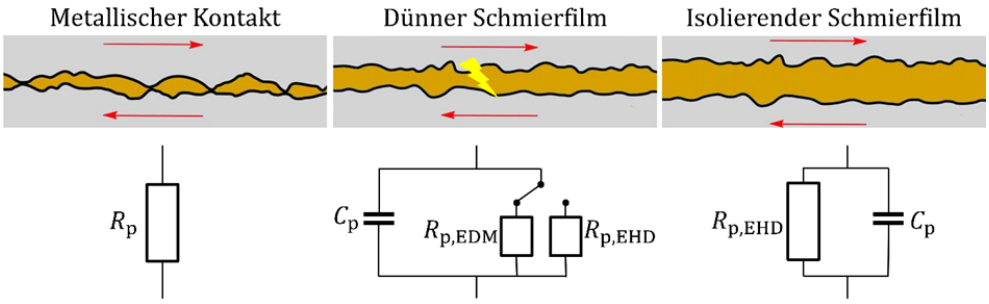

Figure 1. Electrical model of the rolling contact in different lubrication conditions. Reproduced with permission of Reference [14], Copyright ©Elsevier B.V. 2022.

Degradation and Failure Mechanisms of Rolling Bearing

The stressing of rolling bearings can be purely mechanical or with electrical or chemical loads. A purely mechanical loading will sooner or later lead to a failure due to rolling contact fatigue. This failure mechanism has been extensively investigated in the past and a distinction is made between surface and sub-surface initiation. While surface initiated fatigue failures are commonly connected with insufficient lubrication and high shear stresses, sub-surface initiated fatigue will occur even under optimal operating conditions mainly due to pressure induced stress below the surface. The number of bearing failures due to rolling contact fatigue has decreased significantly over time as a consequence of improved materials and optimized lubrication. Instead, other damage patterns have gained importance, particularly failure mechanisms in connection with superimposed electrical stress due to the increased electrification of drive systems [4]. Just as with rolling contact fatigue damage, such damage patterns can be traced back to a surface or sub-surface initiation. The most common surface initiated damage patterns caused by electrical stressing are frosting and fluting beneath the surface, white etching cracks are known to be formed under electrical stressing [15]. Besides these material damage patterns, lubricants can be degraded due to electrical stressing [16]. However, a possible assignment of the damage patterns to typical load variables, such as the current density in a bearing, is challenging. The following section will slightly introduce the damage patterns.

The terms frosting/grey frosting refer to the grey matt appearance of the bearing components affected by the current passage (see Figure 2). FURTMANN [17] describes the cause as short-term melting at the roughness peaks in the rolling contact due to the applied current with repeated over rolling. Macroscopically, the grey frosting resembles a mechanically caused classic grey staining (micropitting). Microscopically, however, there are apparent differences between the rugged fracture edges of micropitting and the soft flowing edges of an electrically-caused grey frosting [17]. According to KRIESE [18], there may be two kinds of crates within the frosted area—smaller melted and flattened or larger and deeper crates where the bearing raceway has been vaporized depending on the energy input. He describes that the small crates are harmless, and the vaporized and deeper crates are more harmful to the bearings. FURTMANN describes the effects in a similar way. Depending on the severity, the raceway changes result in a significant increase in pressure and possibly tear down the lubricant film. Whether melting or vaporization occurs was investigated on ball bearings using variable voltages. In this way, TISCHMACHER [19] could

establish a relationship between melting, vaporization, and the energy level as well as the melting diameter.

Frosting is believed to be a precursor to fluting, which usually leads to increased vibration, wear, and failure [17]. The macroscopic appearance of fluting is shown in Figure 3. According to TISCHMACHER [20], fluting can occur on both the inner and outer rings. At first glance, the fluting pattern appears to be strictly periodic, but on closer inspection, they are revealed as groups of fluting arranged at rolling element distance. Light and dark areas can be recognized, which find their correspondence in valleys and peaks, respectively. While the peaks are characterized by a structure similar to the grey frosting, in the valleys a structure is recognizable that resembles spark-eroded surfaces. TISCHMACHER measured a fluting depth of approximately 3.5 µm and a distance between the fluting tips of roughly 1.3 mm. The Investigations used a grooved ball bearing (Type 6210) with voltage amplitudes between 50 and 150 V and a corresponding bearing current amplitude between 8 and 15 A. The pulse frequency was 2.5 kHz [21]. These bearing raceway changes lead to a degradation of the running operation and a short-term failure [20].

In addition to possible damage to rolling elements and raceways, the electrical stressing also damages the lubricant. The damage manifests itself in a visual change and, above all, in premature aging of the lubricant. The aged lubricant shows poorer lubrication properties accordingly up to a loss of lubrication. Without relubrication, the loss of lubrication leads to direct contact between the rolling partners and thus to wear followed by component failure. The visual appearance of current-damaged/aged oil is shown in Figure 4.

Besides the aforementioned surface and lubricant damage patterns, failure can be initiated beneath the surface. Current passage favors the formation of so-called white etching cracks (WEC). WEC are a more recent damage pattern than typical wear or fatigue damage and can lead to premature bearing failure after 1–20% of the nominal service life L_{10}. Figure 5 shows an inner ring of a cylindrical roller bearing (Type NU206 made of AISI 52100 steel) on the left side, which is affected by current passage. The right side shows the metallography with white etching areas [22].

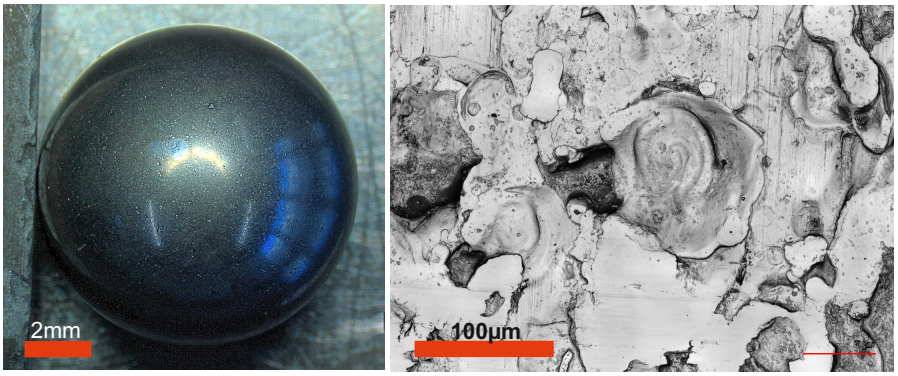

Figure 2. Macroscopic (**left**) and microscopic (**right**) visual appearance of a heavily electrically damaged surface [23].

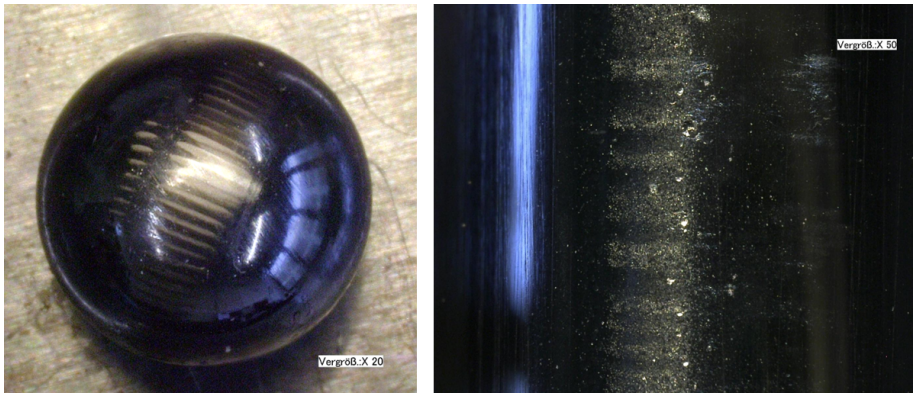

Figure 3. (**left**) Visual appearance of advanced fluting on a bearing ball. (**right**) Fluting at an early stage on a deep groove ball bearing inner ring [23].

Figure 4. Gear oil before (**left**) and after (**right**) the oil was exposed to harmful EDM discharges in a modified bearing test rig.

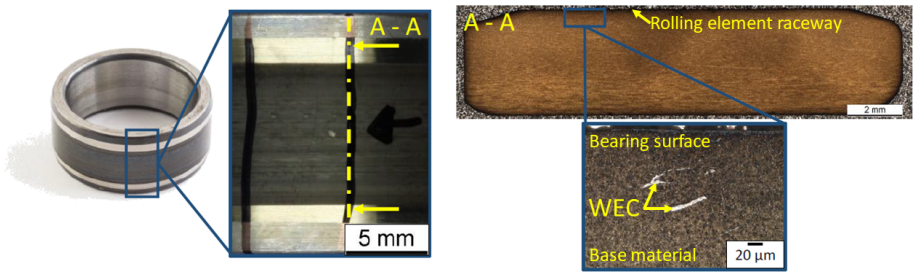

Figure 5. Inner ring of a of a cylindrical roller bearing (Type NU206 made of AISI 52100 steel) affected by current passage (**left**), metallographic analysis after the etching process, showing WEC (**right**) [22].

Even though the damage process itself has not been conclusively clarified, it has been shown that the formation of the WEC is influenced by electrical stressing [15]. For instance, direct current (DC) and alternating current (AC) can lead to WEC. Regarding the lubrication, it makes no difference whether the bearing is oil or grease lubricated [8]. However, the composition of the lubricant can have an influence [15,24]. It was also found that for DC, a higher current or bearing current density (defined as the ratio of the applied current divided by the HERTZ'ian contact area at the operating point) is associated with an earlier occurrence of WEC [8,15,22]. The polarity also influences the formation of WEC: the positively connected bearing component shows a significantly earlier tendency to fail than the negatively one [8,22].

Just as with rolling contact fatigue, the formation of WEC can be broken down to stress exceeding stressability. This could be caused by either higher stresses than expected or

reduced stressability. On the one hand, electrical stressing could therefore influence the formation of WEC by changing the surface and consequently the stress.

On the other hand, a decrease in stressability is most likely to be caused by hydrogen absorption, which in turn can be supported by electrical stress in multiple ways. It has for example been discussed that electrical induced surface erosion or melting could chemically activate the bearing surface. Furthermore, electrical currents could enhance the hydrogen release from a lubricant. Various publications address the different types of electrical stresses. While the non-WEC-related publications focus on the origin and possible influencing parameters of the electrical stresses, the WEC-related publications focus on a correlation between the electrical loading and the damage pattern. An initial overview of the investigated parameter ranges and the observed damage patterns are shown in Table 1. The reader is advised that a direct comparison is not always possible due to the inconsistently used valuation parameters.

Table 1. Overview of electrical stressing of bearings and observed damage patterns.

Source	Electrical Stressing	Bearing Type	Observed Damage Pattern
[25–27]	$0.04 - 3.15$ A/mm^2 $f_{switch} = 3, 8, 10$ kHz	6308, 6309, 6209	Single Frosting, Frosting, Fluting, Lubricant degradation
[28]	$50A$ (AC) at 1.12–2.3 V, $f_{switch} = 10$ Hz	6326, NU230, NU326	Fluting
[18]	450 mio. EDM discharges > 1 A, Temperature 30 °C, 28 days; 900 mio. EDM discharges > 1 A, Temperature 80 °C, 63 days		Frosting Fluting
[28]	$0.075, 0.15, 0.225$ A/mm^2 $f_{base} = 50$ Hz, $f_{switch} = 10$ kHz	four-ball apparatus	Frosting
[29]	$0.5VDC$ $5–6VDC$, 40 µA $2.5VDC$, 25 µA $6–15VDC$, up to 200 µA	6203, NU207	Flaking WEC
[22]	0.01–0.59 A/mm^2 DC 0.1–0.75 A/mm^2 DC	NU206 four-disc apparatus	WEC, Frosting WEC
[15]	0–750 mA DC	Micro Pitting Test rig (MPR)	no WEC: 0–25 mA WEC: 75–250 mA Signs of fluting: 500, 750 mA
[8]	0.01 A/mm^2 0.2–3.9 A/mm^2	NU207 6203	WEC WEC, Frosting

2. Physics of Bearing Currents

Electric motors fed by frequency converters are increasingly used in modern drive systems. In this case, the windings of the motors are not supplied with sinusoidal signals, but with voltage pulses. These approximate a sinusoidal current by alternating the three phase terminals with high frequency (i.e., some 5 kHz) only between the potentials $+0.5U_0$ and $-0.5U_0$. This causes the three output voltages to not add up to zero, so that a common-mode voltage U_{CM} is generated [30]. This voltage results in a parasitic common-mode current I_{CM}, which flows from the stator winding through the capacitance between stator winding and stator core to the stator core and back to the ground. Depending on the geometrical details of the system, the common-mode voltage or common-mode current acts as the cause of the high-frequency bearing currents, classified as electric discharge machining (EDM) or circular bearing current.

EDM bearing currents are caused by the common-mode voltage. They result from the galvanic separation of the stator core, winding and rotor [20]. In the case of fully lubricated

bearings, the common-mode voltage U_{CM} injected into the stator winding splits along a capacitive voltage divider across the entire drive system, as shown in Figure 6a. The resulting electrical voltage across the bearings is calculated using the bearing voltage ratio:

$$f_{BVR} = \frac{C_{WR}}{C_{WR} + C_{RS} + C_{b1} + C_{b2} + C_{b3} + \left(\frac{C_g \cdot (C_{b4} + C_{b5})}{C_g + C_{b4} + C_{b5}}\right)}, \tag{1}$$

which results in a bearing voltage of:

$$U_b = U_{CM} \cdot f_{BVR}. \tag{2}$$

The circular bearing current is caused by the common-mode current if the bearings are conductive due to mixed friction or an EDM breakdown. Depending on the common-mode impedance $\underline{Z}_{CM}$ corresponding to the common-mode voltage $\underline{U}_{CM}$, this causes the common-mode current

$$\underline{I}_{CM} = \frac{\underline{U}_{CM}}{\underline{Z}_{CM}}. \tag{3}$$

This creates a circular magnetic field in the stator yoke [30] with impedance $\underline{Z}_S$, which induces a voltage in the shaft:

$$\underline{U}_{shaft} = \underline{Z}_S \cdot \underline{I}_{CM}. \tag{4}$$

In the standard case, this shaft voltage drives a current in the conductor loop consisting of bearings, the bearing shields, the laminated stator core, the housing, the shaft, and the rotor, which is drawn with the solid green line in Figure 6b. The circular bearing current,

$$\underline{I}_{circ} = \frac{\underline{U}_{shaft}}{\underline{Z}_{total}}, \tag{5}$$

depends on the shaft voltage U_{shaft} and the impedance of the bearing current path $\underline{Z}_{total}$. Depending on the design of the overall system consisting of motor, bearings, and gear unit, other paths for circular bearing currents are possible in addition to this standard path. These are shown as examples in Figure 6b as dashed lines.

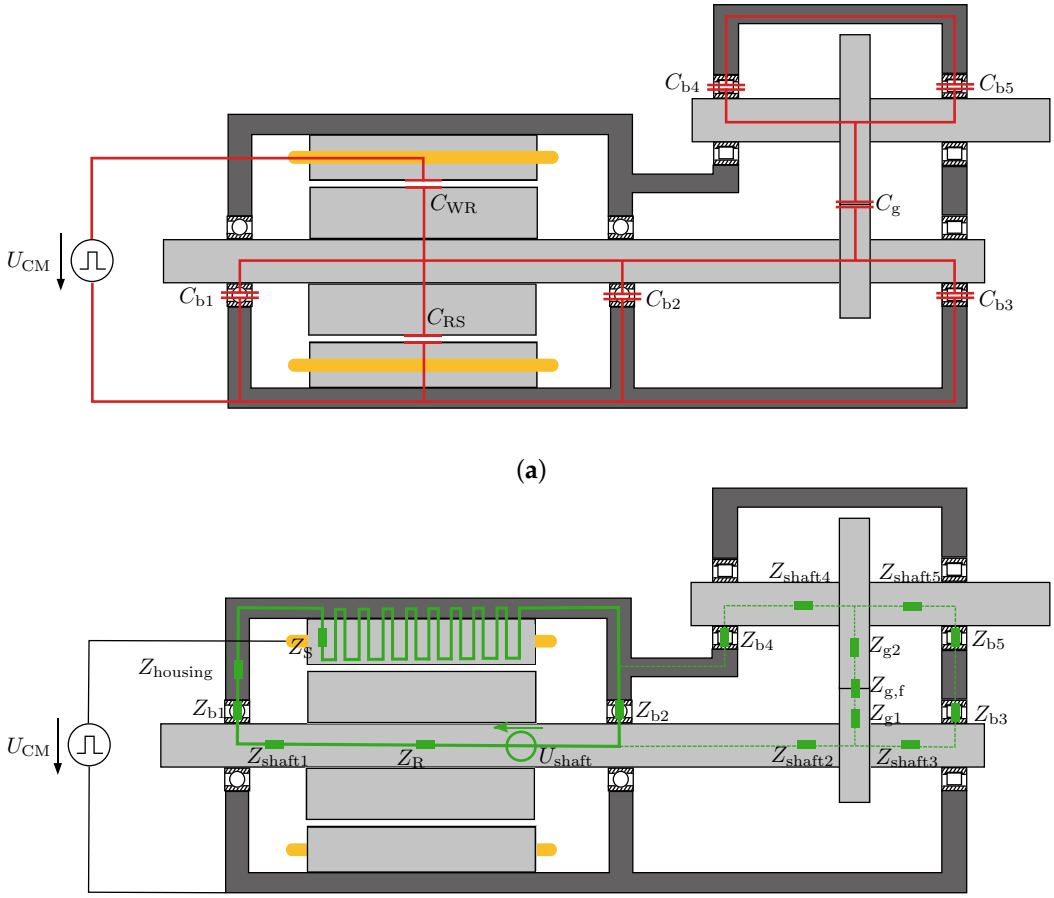

Figure 6. EDM und circular bearing currents.

3. System Modeling

To avoid the damage patterns introduced by the bearing currents mentioned, suitable prevention mechanisms for the drive system, consisting of the inverter, the machine, and the gearbox, must be selected in the design stage. For this purpose, various approaches to predicting bearing currents have been developed, which are mostly limited to an electrical machine [25,31,32]. If only the rolling bearing is considered, the use of hybrid bearings seems to be a suitable countermeasure to solve harmful bearing currents [33]. The previous section, on the other hand, has shown that the parasitic bearing currents can flow through the entire drive system according to the distribution of electrical impedance in it and thus may also cause damage to the gear unit. With this knowledge, it becomes clear that the use of, e.g., hybrid bearings, only displaces the problem, which can subsequently lead to current-related damage elsewhere in the overall system (see Figure 7). Therefore, to predict the potential electrocorrosion, it is necessary to model an electrical equivalent circuit for the entire system.

An approach to describe the dependencies between the machine elements in an entire electrical drive system was developed by FURTMANN [12], in which a simulation model of a drive system consisting of an electric motor and a gearbox was created. The model made it possible to test countermeasures for their effectiveness in preventing or reducing EDM discharges. Figure 7 shows the effect of insulations or conductive paths at various locations in a drive system on the resulting voltage distribution. It is apparent that by solving a problem in one place (e.g., by replacing steel rolling element bearings with hybrid bearings in the electric motor), there will be a shift to and even an increase in voltage elsewhere. In

addition to the electric machine and the gearbox, the effects of the inverter and the cables must be taken into account when calculating the electrical bearing load [34].

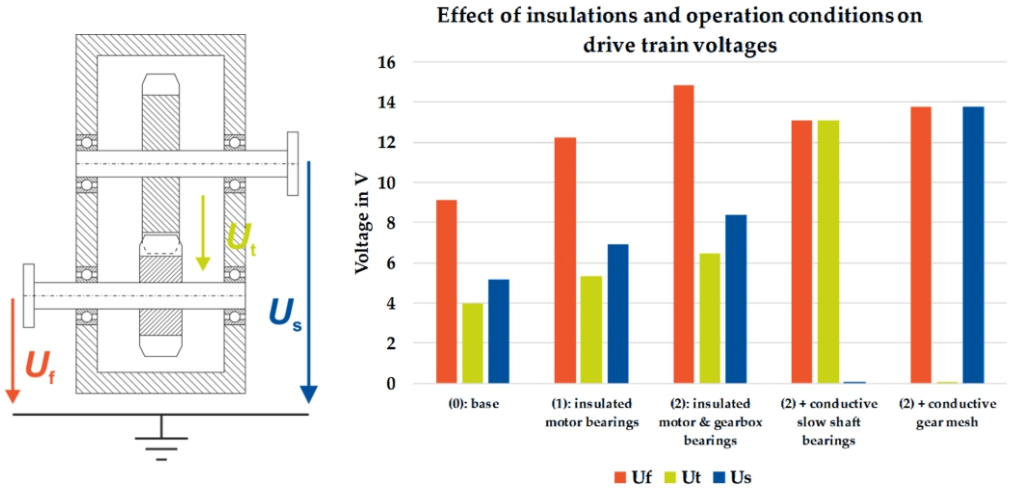

Figure 7. Effect of insulations and conductive path on voltage distribution in an electrical drive system. According to [13].

3.1. Electrical Machine Model

The modeling of an electrical machine as part of a drive system, to predict electro-corrosion, can be divided into two parts. First, a model to calculate the common-mode impedance Z_{CM} over a wide frequency range is needed, so that Equation (3) can be used to determine the common-mode current, as it is the cause of circular bearing currents. Here, different models are presented in the literature. First efforts were made with lumped parameter models for the high-frequency behavior prediction of an electrical machine, as given in [35,36], but they are useless for prediction in the design stage because the identification of the parameters in the proposed equivalent circuit is based on measurements. Further, multi-conductor-transmission line models, such as those presented in [30,32,37–39], are widely accepted for modeling high-frequency machine behavior. According to the multi-conductor-transmission line, a conductor i coupled with a conductor j is modeled, as shown in Figure 8, by a self-resistance R_{ii}, a self-inductance L_{ii}, a capacitance C_g to ground, a capacitance C_k to conductor j, and a resistance R_g and resistance R_{CM} representing dielectric losses, which are usually neglected. Consequently, a machine can be described by distributed parameters per coil or turn. Additionally, current and field displacement is taken into account by adding inter-wire coupling equations. The corresponding parameters can be identified analytically or by finite-element method (FEM) simulations instead of measurements and thus can be used for prediction in the design stage. Unfortunately, the identification is often restricted to a single slot, because inter-wire couplings between conductors in neighboring slots are considered to be negligible due to the shielding effect of the stator core [40]. However, as a consequence of the decreasing iron permeability with increasing frequency, the magnetic flux crosses slots, so that the couplings across a slot are not negligible at high frequencies, as [41] state. Thus, only a model such as that presented in [42], which includes all relevant inter-wire couplings, provides acceptable results for the common-mode impedance Z_{CM}.

Second, the conducting path in which the bearing current flows needs to be modeled. Therefore, the impedances of the system—mainly capacitive for EDM and mainly inductive for circular bearing currents—need to be calculated. If a bearing current only flows in the assumed standard path, a restriction to a machine model is sufficient. Such a model with corresponding calculation methods can be found in [20,25,43]. Unfortunately, the current flow can extend beyond the machine boundaries, so other components of the system are affected too. To predict the potential stress due to current flow, the current divider must be

correctly represented in the overall system. Hence, the equivalent circuit of the standard path needs to be extended by the further components, e.g., the bearings and the gear unit.

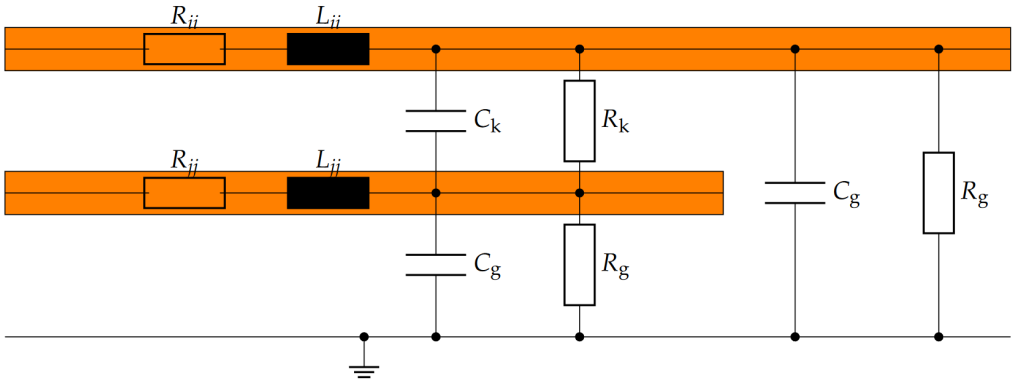

Figure 8. Multi-conductor-transmission line model for modeling an electrical machine at high frequencies. According to [42].

3.2. Electric Behavior Modeling of Rolling Bearings

This section summarizes the current state of research regarding the electrical behavior of rolling contacts.

3.2.1. Capacitance

In a highly loaded elastohydrodynamic contact in full lubrication conditions, as in rolling bearings or gear contacts, two electrically conductive bodies are located opposite to each other, separated by a thin lubricating film. In this case, the bodies can be considered as capacitor plates with a defined area and distance and the lubricant as a dielectric. The capacitance of a model contact can be determined assuming an elastohydrodynamic lubrication (EHL) contact as a plate capacitor:

$$C = \varepsilon \cdot \frac{A}{d}, \tag{6}$$

where $\varepsilon = \varepsilon_0 \cdot \varepsilon_r$ is the absolute permittivity of lubricants, A the HERTZ'ian contact area, and d is the film thickness between both bodies. Due to the simplification of the real geometry to the HERTZ'ian area (6), for instance [17,25,44,45] modified the capacitance model (6) by either introducing additive or multiplicative corrections to better fit the model prediction to the capacitance measured. This includes the influence of the regions outside the HERTZ'ian contact zone with the capacitance $C_{outside}$ (see Figure 9). To simplify the calculation, it is assumed that the inlet zone is filled with lubricant. In the outlet zone, the lubricant separates evenly on the rolling element and raceway. Assuming this, the total capacitance is then the sum of the HERTZ'ian contact capacitance and the capacitance of the surrounding regions, while C_{Hertz} may be approximated by:

$$C_{Hertz,h_c} = \varepsilon_0 \cdot \varepsilon_r \cdot \frac{A_{Hertz}}{h_c}, \tag{7}$$

assuming the film thickness inside the HERTZ'ian contact zone is equal to the central film thickness h_c. This value can be calculated, e.g., with HAMROCK–DOWSONS [46] set of equations for point contacts. These are based on dimensionless parameters for speed U, load W, material G and geometry k_e.

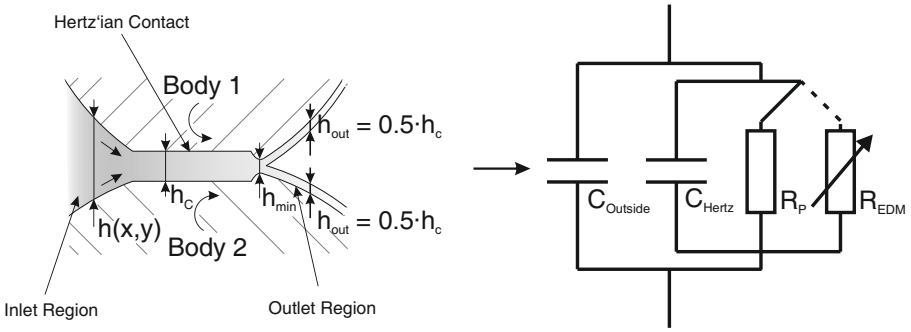

Figure 9. Electrical analogy model of an EHL contact. Adopted from [17,47].

It must be considered that the proportion of $C_{outside}$ is usually larger than C_{Hertz} [17,48,49]. $C_{outside}$ varies with contact geometry and h_c, and it is usually taken into account in the total capacitance determination of a contact $C_{tot,con}$ through a factor k_c

$$k_c = \frac{C_{tot,con}}{C_{Hertz,h_c}}, \tag{8}$$

which indicates the ratio between the total capacitance and the capacitance of the HERTZ'ian contact for a given contact. An ideal k_c factor would then take into account the effect of the deformations of the bodies outside the HERTZ'ian contact zone as well as the influence of the real film thickness distribution inside the HERTZ'ian contact on the total capacitance. To consider the contribution of the capacitance outside the HERTZ'ian zone, BARZ [50] and WITTEK [51] used a universal value of $k_c = 3.5$ giving a good approximation for axially loaded rolling bearings. However, $C_{outside}$ is a function of film thickness and JABLONKA ET AL. [49] showed that k_c increases almost linearly as a function of film thickness for a model EHL contact. For a radially-loaded bearing, the rolling elements have different k_c values due to varying load distributions. In his work, FURTMANN developed a method for empirically determining the k_c-factor based on extensive test results as a function of the lubricant film height [17]. In [47,52], SCHNEIDER ET AL. derived a solely analytical equation to calculate the k_c-factor based only on the dimensionless parameters introduced by HAMROCK–DOWSONS [46]. The equation represents a curve fit of representative simulation results. The simulations were conducted with an EHL solver based on the work of LUBRECHT and VENNER [53,54]. It is based on a multigrid-method to solve the coupled Reynolds equation that takes the surface elastic deformation and load balance into account. The simulations were conducted for a wide range of the aforementioned dimensionless parameters (U, G, W, k_e). An exemplary film thickness distribution inside the HERTZ'ian contact obtained from the multigrid method is shown in Figure 10. It is seen that no uniform film thickness can be assumed in the area of the HERTZ'ian contact.

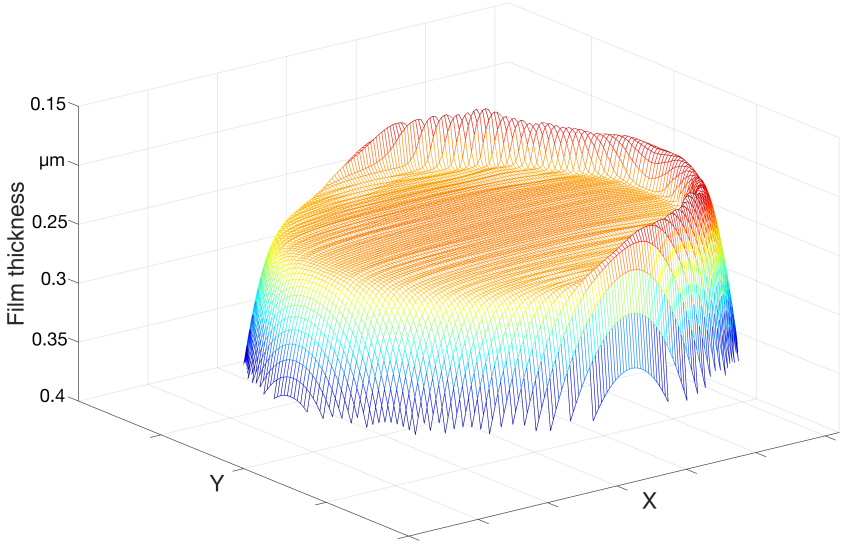

Figure 10. Resulting film thickness of the multigrid method. The area is shown inverted for better illustration.

3.2.2. Impedance

If the electrical field strength in the lubrication gap rises beyond the breakdown field strength of the lubricant, the equivalent circuit shown in Figures 9 and 11 is obtained. Below the critical voltage, the contact behaves like a capacitance with a large parallel resistance R_p. When the threshold voltage of the lubricated gap is exceeded and a discharge happens, the circuit switches over and the capacitor can be discharged via the resistor R_{EDM}. The magnitude of the discharge resistor is time-varying [25,55,56].

In the case where no discharges occur, the internal resistance R_P of the lubricant has to be calculated additional to the capacitance of a contact [57,58]. The determination of R_p is analog to the assumptions of the capacitance calculation and the results in (9) by taking the lubricant specific resistance ρ into account. Here, the HERTZ'ian contact area is also used as a calculable basis. The influence of the areas outside the HERTZ'ian contact area k_r corresponds to the reciprocal value of the k_c factor [45]:

$$R_p = k_r \frac{\rho \cdot h_c}{A_{Hertz}}. \tag{9}$$

The impedance of a single contact then depends on the electrical frequency f, the contact capacitance $C_{tot,con}$ and the lubricant inner resistance $R_{parallel}$:

$$\underline{Z}_{tot,con} = \frac{R_p \cdot \frac{1}{\mathrm{j}2\pi f C_{tot,con}}}{R_p + \frac{1}{\mathrm{j}2\pi f C_{tot,con}}}. \tag{10}$$

The impedance of a rolling element is then the series connection of the inner and the outer ring contact. The internal impedance of the rolling element is usually neglected because it is very small [45]:

$$\underline{Z}_{re} = \underline{Z}_{tot,con,ir} + \underline{Z}_{tot,con,or}. \tag{11}$$

Looking at a complete bearing, the rolling elements are connected in parallel, see Figure 11. Assuming a total of Z rolling elements, the total bearing impedance $\underline{Z}_b$ would result in:

$$\frac{1}{\underline{Z}_b} = \sum_{i=1}^{Z} \frac{1}{\underline{Z}_{re,i}}. \tag{12}$$

FURTMANN discussed the influence of the cage on the total impedance and concluded that the deviation by modeling the cage as ideally conducting compared to an insulating cage as assumed in Equation (12) is small [17]. This is primarily due to the ratio of inner and outer contact impedance being similar for all rolling elements, which leads to similar potentials on all rolling elements.

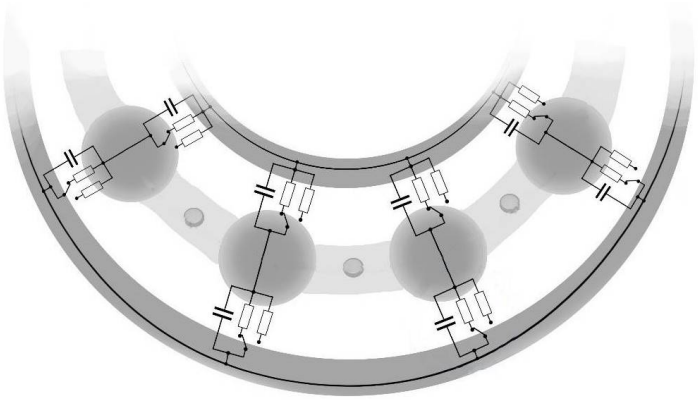

Figure 11. Electrical equivalent circuit assuming an insulating cage.

3.2.3. Electrical Properties of Lubricant

To model the electrical behavior of a bearing, knowledge of the electrical lubricant characteristics is mandatory [16,56,58–60]. The most important characteristic values are the dielectric strength E [17,61], the relative permittivity ε_r [31,44,51,56,62] and the electrical specific resistivity ρ [16,58,60]. Both the capacitance and impedance calculation rely greatly on the predictability of the electrical lubricant properties. The relative permittivity is an important factor for calculating the electrical capacitance. Since the electrical properties depend strongly on pressure and temperature, as shown in Figure 12 [63], the methods underlying the estimation of these are of high importance. For example, to describe dielectric conductivity as a function of temperature and pressure, the modified CLAUSIUS–MOSSOTTI equation is well established [64–66] but tends to have strong deviations under high pressures in direct comparison to measurements as shown by FURTMANN [17].

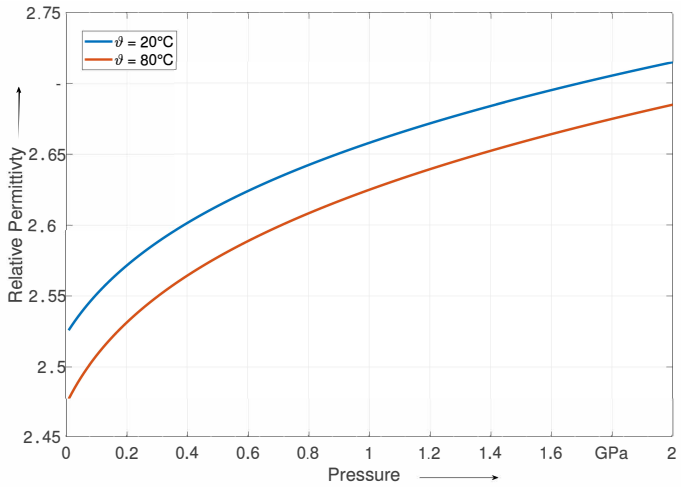

Figure 12. Pressure and temperature dependent relative permittivity using the BODE equations.

Another possible approach is based on measurements from a high pressure quartz-viscometer. Together with a set of equations provided by BODE [67,68], it is also possible to describe the temperature and pressure dependent rheological and electrical properties of the lubricant.

Both methods presuppose the knowledge of the reference density ϱ_0 and of the reference relative permittivity ε_{r0}. The reference density at 15 °C is usually provided in the lubricant data sheet and the reference relative permittivity can be determined experimentally at ambient pressure, e.g., as done by WITTEK [62].

4. Sensorial Use of Rolling Bearings

In the context of Industry 4.0 the demand for data of technical systems and processes is on a constant rise [69]. The acquisition of these data can be realized in various ways, whereas the data quality varies especially with the choice of measurands and sensor positions [70]. A promising approach to measure data close to the process is the use of sensing machine elements (SME), which build upon the primary mechanical functions of conventional machine elements and extend their functionality in terms of sensor functions [71]. In the following, two approaches to utilize rolling bearings sensorially are described.

4.1. Bearings as Load Sensors

An inevitable basis for sensor bearings is the understanding and modeling of all relevant factors on the electrical properties of rolling bearings. In the late 1950s, the capacitive method made its entry in the race of measuring lubrication film thicknesses of rolling contacts to develop formulas that would allow a reliable prediction of rolling bearing's lubrication condition [72–75]. Up to today, capacitive lubrication film thickness measurements are carried out and improved to further study steel on steel contacts in the EHL regime [49,51,76,77]. Further studies are carried out in order to understand, model and predict the electrical behavior of rolling element bearings [47,52,76,78,79]. This improved electric modeling of rolling bearings and affordable measurement devices make the sensorial use of rolling bearings possible [80,81].

As seen in Equation (7), the bearing's capacitance and therefore impedance depends on the lubrication film thickness and the HERTZ'ian area. A rising load causes the film thickness to decrease and the HERTZ'ian area to increase. Both contribute to a rising capacitance and decreasing impedance, which can be measured by contacting the inner and outer ring of a rolling bearing. Besides measuring the capacitance, further parameters need to be monitored to calculate the bearing load. The oil temperature has a significant influence on the lubricant's viscosity and consequently on the lubrication film thickness, and therefore needs to be measured. The shaft's rotational speed also influences the film thickness, but can be determined from the impedance signal without the need for an extra speed sensor [82].

Ultimately, the bearing load can be calculated, resulting in a sensorial rolling bearing which is an SME with the potential to be integrated into the majority of mechanical machines even with the option to be retrofitted in existing machines, requiring an insulation of at least one bearing ring and an electric connection to the rotating ring, e.g., via a slip ring [83]. Monitoring the load on bearings allows an improved prediction of the remaining useful lifetime and therefore contributes to maximizing the utilization of components' actual lifetime. At the same time, a combination with failure monitoring using the electric impedance is possible to limit the risk of downtime due to premature failure [83].

4.2. Detection of Roller Bearing Damage by Impedance Measurement

Although rolling bearings have a limited durability, only 0.5% of them fail before their estimated operation time [84]. However, on the other hand, rolling bearing damages cause 20% of machine failures [85]. In the case of motor spindles, bearing damages are accountable for nearly 37% of their breakdowns [86]. An early detection of rolling bearing failures can therefore reduce unplanned downtimes of machines and increase their reliability.

Methods for rolling bearing damage early detection include measuring acoustic emission [87], analysis of the instantaneous angular speed (IAS) of the shaft [88], and vibration monitoring plus temperature measurement, which are the most common methods [85].

It measures the vibration excitation resulting from overrolling surface damages on the raceways or on the rolling elements [85]. The disadvantage of these measurement methods is that the used sensors are often located far away from the supervised component. This causes uncertainties in measurement. They can be reduced by placing sensors as close as possible to the observed component, which is realized best by in situ applications, where machine elements themselves are used as sensors [89]. Because of their electrical behavior under alternating current, impedance measurements of rolling bearings can be used for failure monitoring and remaining useful life prediction, as mentioned above [83].

It could be shown that changes in the impedance signal display arising bearing damage. Figure 13 illustrates the impedance signal of a fatigue test. So-called fast pikes occur in all stages of the bearing life. They are generated by surface asperities. Their number decreases over the operating time and is constantly lower than in a run-in phase until an initial damage appears. After its occurrence, the number and height of peaks are higher than in the run-in. When the damage progresses, the fast peaks appear at the beginning and the end of a surface defect. So, it is possible not only to diagnose the attendance of a surface failure but also to determine its elongation in the raceway. It could also be shown that it is possible to determine whether the damage is on the inner, the outer ring, or on the rolling elements from an impedance signal [14].

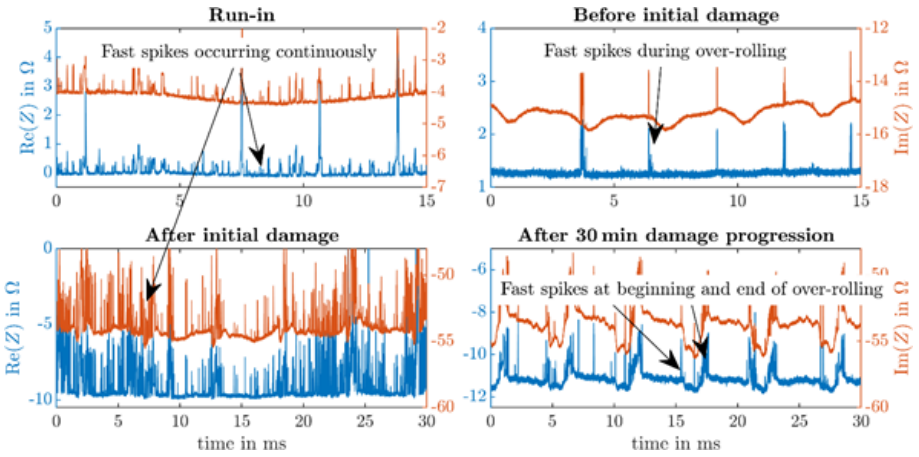

Figure 13. Impedance measurements at different stages of the bearing life. Reproduced with permission of Reference [14], Copyright ©Elsevier B.V. 2022.

Current research focuses on the early detection of bearing failures by measuring their impedance and calculating statistical features from the signal. Earlier investigations displayed changes in the impedance signal, the standard deviation, and the kurtosis over the bearing operating life [90]. This motivates the hypothesis of early damage detection by impedance measurement, which has to be investigated further.

5. Conclusions

Rolling bearings face different damaging effects. Besides mechanical effects, current-induced bearing damage occurs in electrical drive systems. Therefore, it is of increasing interest to understand the differences leading to known electrical damage patterns, e.g., frosting, fluting, and WEC. Understanding the underlying physical effects allows the generation of models to predict the possibility of bearing currents during the design of electro-mechanical drive systems. Section 2 displays how an electrical machine can be modeled to calculate the voltage across the bearings from the common-mode voltage generated by frequency converters. This bearing voltage ratio, in return, depends not only on the geometry and electrical properties of the motor but also on the bearings' impedance, as shown in Section 3. In addition, basic modeling of the bearings' impedance was shown, which in return depends on geometry, loads, and lubricant properties, among others. It turns out that the prediction of bearing currents requires close interaction of models on

different scales—the contact between rolling elements and bearing races with a lubrication film and surface roughness on a sub-micrometer scale via the whole bearing, its dynamics, and load distribution on a centimeter scale, to the whole electrical machine, and even the whole drive system, including the frequency converter, as well as a transmission and following components.

Bearing voltages may not always be an unintended effect of frequency converters but can be deliberately applied to measure the bearing's impedance, which holds the opportunity for rolling bearing damage early detection and estimating bearing loads for the prediction of mechanical damage. To do so, it is necessary to differentiate between damaging and non-damaging currents, which is still part of the current research, especially for WEC. Because surface damage can be detected and measured by impedance gauging, it can be used for discovering electrically caused damage as well. For electrical damage prediction, it is currently not clear if impedance measurement is sufficient. The current state of research shows that the surfaces have to be damaged already to change the impedance signal. To identify operating conditions that lead to WEC and other electric damaging effects, the whole drive system and its components have to be modeled and investigated further. So, a deeper knowledge about the electrical behavior of the single contact zone up to the whole machine element and the complex drive system is necessary.

6. Outlook

While individual models in their respective scales, such as lubrication film, bearing, electrical machine, and drive systems, have become increasingly elaborate in recent years of research, the combination of these models still has a high potential for a deeper understanding of the entire system. Therefore, more methodical approaches for developing cross-scale models would be appropriate in this context. Furthermore, additional experimental and simulative research is needed for a service life estimation of single machine elements and drive systems under mechanical and electric loads. The general impedance behavior of mechanical bearing damage must be described and understood more deeply, especially in the context of damage prediction. For instance, the detection of surface roughening due to electrical damage by impedance measurement is part of current research. The investigation of factors influencing the electrical damage degree is also interesting, primarily for damage prediction and modeling the behavior of the involved components to simulate their performance in the drive system and as single machine elements. These simulations can help develop a broader understanding of the influence of bearing currents on WEC.

Author Contributions: Conceptualization, V.S., C.B., P.H., D.C., F.M.B.-D., S.P. and F.G.G.; methodology, V.S., C.B. and P.H.; software, V.S., C.B., P.H. and D.C.; validation, V.S., C.B. and P.H.; formal analysis, V.S., C.B. and P.H.; investigation, V.S., C.B., P.H., D.C., F.M.B.-D., S.P. and F.G.G.; data curation, V.S., C.B., P.H., D.C. and F.G.G.; writing—original draft preparation, V.S., C.B., P.H., D.C., F.M.B.-D., S.P. and F.G.G.; writing—review and editing, V.S., C.B., P.H., D.C., F.M.B.-D., S.P. and F.G.G.; visualization, V.S., C.B., P.H., D.C., F.M.B.-D. and S.P.; supervision, F.G.G., B.P., G.J. and E.K.; project administration, F.G.G., B.P., G.J. and E.K.; funding acquisition, F.G.G., B.P., G.J. and E.K. All authors have read and agreed to the published version of the manuscript.

Funding: This research was funded by Otto von Guericke Research Association (AiF) grant number 22079 N and by the Deutsche Forschungsgemeinschaft (DFG, German Research Foundation)—467849890; 463357020.

Institutional Review Board Statement: Not applicable.

Informed Consent Statement: Not applicable.

Data Availability Statement: Data is contained within the article.

Acknowledgments: In this section you can acknowledge any support given which is not covered by the author contribution or funding sections. This may include administrative and technical support, or donations in kind (e.g., materials used for experiments).

Conflicts of Interest: The authors declare no conflict of interest.

Nomenclature

The following abbreviations are used in this manuscript:

Greek Symbols		
ϵ	absolute permittivity	F/m
ϵ_0	vacuum permittivity $= 8.8541878 \times 10^{-12}$	A·s/V·m
ϵ_r	relative permittivity	−
ρ	density	S/m
ϱ	specific resistance	kg/m^3
Roman Symbols		
A	area	m^2
C	capacitance	F
d	thickness of gap between capacitor plates	m
E	dielectric strength	V/m
f	frequency	Hz
f_{BVR}	bearing voltage ratio	
h	film thickness	m
I	current	A
k_c	ratio between C_{total} and C_{Hertz,h_c}	−
k_r	ratio between R_{total} and R_{Hertz,h_c}	−
L	inductance	H
R	resistance	Ω
U	voltage	V
Z	impedance	Ω
j	imaginary unit	
Subscripts		
0	reference	
b	bearing	
BVR	bearing voltage ratio	
c	central	
circ	circular	
CM	common mode	
con	contact	
EDM	electrical discharge machining	
EHL	elastohydrodynamic lubrication	
g	gear	
g, f	gear, film	
housing	housing	
ir	inner raceway	
or	outer raceway	
p	parallel	
R	rotor	
re	rolling element	
RS	rotor stator	
rs	replenishment/starvation	
S	stator	
shaft	shaft	
tot	total	
total	total bearing current path	
WR	winding rotor	
x	x-direction	
y	y-direction	
j	jth rolling element	

References

1. Pittroff, H. Wälzlager im elektrischen Stromkreis: Riffelbildung infolge von Stromdurchgang. *WäLzlagertechnische Sonderschriften* **1968**, *95*, 54–61.
2. Pöhlmann, A. *Wälzlager in Elektrischen Lokomotiven und Diesellokomotiven*; SKF Kugellagerfabriken Schweinfurt: Schweinfurt, Germany, 1959.
3. Schenk, O. Korrosionsformen bei Wälzlagern. *Maschinenschaden* **1954**, *27*, 151–156.
4. Habibullah, M.; Lu, D.D.; Xiao, D.; Rahman, M.F. Finite-State Predictive Torque Control of Induction Motor Supplied From a Three-Level NPC Voltage Source Inverter. *IEEE Trans. Power Electron.* **2017**, *32*, 479–489. [CrossRef]
5. Hausberg, V. Elektrische Lagerbeanspruchung Umrichtergespeister Induktionsmaschinen. Ph.D. Thesis, Leibniz Universität Hannover, Hannover, Germany, 2001.
6. Plazenet, T.; Boileau, T.; Caironi, C.C.; Nahid-Mobarakeh, B. Influencing Parameters on Discharge Bearing Currents in Inverter-Fed Induction Motors. *IEEE Trans. Energy Convers.* **2021**, *36*, 940–949. [CrossRef]
7. Peta, K.; Bartkowiak, T.; Galek, P.; Mendak, M. Contact Angle Analysis of Surface Topographies Created by Electric Discharge Machining. *Tribol. Inter.* **2021**, 107–139. [CrossRef]
8. Loos, J.; Bergmann, I.; Goss, M. Influence of High Electrical Currents on WEC Formation in Rolling Bearings. *Tribol. Trans.* **2021**, *64*, 708–720. [CrossRef]
9. von Jouanne, A.; Collin, R.; Stephens, M.; Miao, Y.; Thayil, B.; Li, C.; Agamloh, E.; Yokochi, A. Motor Bearing Current Characterization in SiC- Based Variable Frequency Drive Applications. In Proceedings of the 2020 IEEE Energy Conversion Congress and Exposition (ECCE), Detroit, MI, USA, 11–15 October 2020; pp. 2718–2725. [CrossRef]
10. He, F.; Xie, G.; Luo, J. Electrical Bearing Failures in Electric Vehicles. *Friction* **2020**, *8*, 4–28. [CrossRef]
11. Prashad, H. Theoretical Analysis of Capacitive Effect of Roller Bearings on Repeated Starts and Stops of a Machine Operating Under the Influence of Shaft Voltages. *J. Tribol.* **1992**, *114*, 818–822. [CrossRef]
12. Furtmann, A.; Tischmacher, H.; Poll, G. Extended HF Equivalent Model of a Drive Train. In Proceedings of the 2016 XXII International Conference on Electrical Machines (ICEM), Piscataway, NJ, USA, 4–7 September 2016; pp. 2244–2250. [CrossRef]
13. Furtmann, A.; Poll, G. Electrical Stress and Parasitic Currents in Machine Elements of Drive Trains with Voltage Source Inverters. In Proceedings of the International Conference on Gears, Garching, Germany, 13–15 September 2017.
14. Martin, G.; Becker, F.M.; Kirchner, E. A Novel Method for Diagnosing Rolling Bearing Surface Damage by Electric Impedance Analysis. *Tribol. Int.* **2022**, *170*, 107503. [CrossRef]
15. Gould, B.; Demas, N.; Erck, R.; Lorenzo-Martin, M.C.; Ajayi, O.; Greco, A. The effect of electrical current on premature failures and microstructural degradation in bearing steel. *Int. J. Fatigue* **2021**, *145*, 106078. [CrossRef]
16. Preisinger, G. Cause and Effect of Bearing Currents in Frequency Converter Driven Electrical Motors: Investigations of Electrical Properties of Rolling Bearings. Ph.D. Thesis, TU Wien, Vienna, Austria, 2002.
17. Furtmann, A. Elektrische Belastung von Maschinenelementen im Antriebsstrang. Ph.D. Thesis, Leibniz Universität Hannover, Hannover, Germany, 2017.
18. Kriese, M.; Wittek, E.; Gattermann, S.; Tischmacher, H.; Poll, G.; Ponick, B. Influence of bearing currents on the bearing lifetime for converter driven machines. In Proceedings of the Influence of Bearing Currents on the Bearing Lifetime for Converter Driven Machines, Marseille, France, 2–5 September 2012; pp. 1735–1739. [CrossRef]
19. Tischmacher, H.; Gattermann, S. Bearing currents in converter operation. In Proceedings of the XIX IEEE International Conference on Electrical Machines-ICEM 2010, Rome, Italy, 6–8 September 2010; pp. 1–8. [CrossRef]
20. Tischmacher, H. Systemanalysen zur Elektrischen Belastung von Wälzlagern bei Umrichtergespeisten Elektromotoren. Ph.D. Thesis, Leibniz Universität Hannover, Hannover, Germany, 2017.
21. Tischmacher, H.; Gattermann, S. Multiple Signature Analysis for the Detection of Bearing Currents and the Assessment of the Resulting Bearing Wear. In Proceedings of the International Symposium on Power Electronics Power Electronics Electrical Drives, Automation and Motion, Sorrento, Italy, 20–22 June 2012; pp. 1354–1359. [CrossRef]
22. Gutiérrez Guzmán, F.; Özel, M.O.; Pinard, P. *Risse auf Lagerringen-707 II*; Forschungsvereinigung Antriebstechnik e.V.: Frankfurt am Main, Germany, 2017; p. 1229.
23. Schneider, V.; Stockbrügger, J.O. *Stromdurchgang am Wälzlager-863 I*; Forschungsvereinigung Antriebstechnik e.V.: Frankfurt am Main, Germany, 2022; p. 1501.
24. Iso, K.; Yokouchi, A.; Takemura, H. *Research Work for Clarifying the Mechanism of White Structure Flaking and Extending the Life of Bearings*; SAE Technical Paper 2005-01-1868; SAE Technical Paper: Warrendale, PA, USA, 2005. [CrossRef]
25. Mütze, A. Bearing Currents in Inverter-Fed AC-Motors. Ph.D. Thesis, Technische Universität Darmstadt, Darmstadt, Germany, 2004.
26. Muetze, A.; Binder, A.; Vogel, H.; Hering, J. Experimental evaluation of the endangerment of ball bearings due to inverter-induced bearing currents. In Proceedings of the Conference Record of the 2004 IEEE Industry Applications Conference, 39th IAS Annual Meeting, Seattle, WA, USA, 3–7 October 2004; pp. 1989–1995. [CrossRef]
27. Muetze, A.; Binder, A.; Vogel, H.; Hering, J. What can bearings bear? *IEEE Ind. Appl. Mag.* **2006**, *12*, 57–64. [CrossRef]
28. Graf, S.; Sauer, B. (Eds.) *Surface Mutation of the Bearing Raceway during Electrical Current Passage in Mixed Friction Operation*; VDMA: Frankfurt am Main, Germany, 2020.

29. Plazenet, T.; Boileau, T. Overview of Bearing White Etching Cracks due to Electrical Currents. In Proceedings of the 2021 IEEE 13th International Symposium on Diagnostics for Electrical Machines, Power Electronics and Drives (SDEMPED), Dallas, TX, USA, 22–25 August 2021; pp. 440–446. [CrossRef]
30. Muetze, A.; Binder, A. Generation of High-Frequency Common Mode Currents in Machines of Inverter-Based Drive Systems. In Proceedings of the 2005 European Conference on Power Electronics and Applications, Dresden, Germany, 11–14 September 2005. [CrossRef]
31. Kriese, M.; Wittek, E.; Gattermann, S.; Tischmacher, H.; Poll, G.; Ponick, B. Prediction of Motor Bearing Currents for Converter Operation. In Proceedings of the XIX International Conference on Electrical Machines—ICEM, Rome, Italy, 6–8 September 2010; pp. 1–6. [CrossRef]
32. Magdun, O. Calculation of High-Frequency Current Distribution in Inverter-Fed Electrical Machines. Ph.D. Thesis, Darmstadt University of Technology, Darmstadt, Germany, 2013.
33. Huan, J.; Li, S.; Xia, Z.; Wang, Y.; Wang, W.; Shi, G. Experimental Study on Electric Corrosion Damage of Bearing and Solution. *Proc. Inst. Mech. Eng. Part C J. Mech. Eng. Sci.* **2022**. [CrossRef]
34. Busse, D.; Erdman, J.; Kerkman, R.; Schlegel, D.; Skibinski, G. System Electrical Parameters and Their Effects on Bearing Currents. *IEEE Trans. Ind. Appl.* **1997**, *33*, 577–584. [CrossRef]
35. Boglietti, A.; Carpaneto, E. An Accurate Induction Motor High- Frequency Model for Electromagnetic Compatibility Analysis. *Electr. Power Components Syst.* **2001**, *29*, 191–210. [CrossRef]
36. Grandi, G.; Casadei, D.; Reggiani, U. Common- and Differential-Mode HF Current Components in AC Motors Supplied by Voltage Source Inverters. *IEEE Trans. Power Electron.* **2004**, *19*, 16–24. [CrossRef]
37. Helmholdt-Zhu, T.; Knebusch, B.; Borcherding, H. High-Frequency Models for the Prediction of Transient Effects in Motor Windings under Fast Rising Impulse Voltages. In Proceedings of the PCIM Europe Digital Days 2020, International Exhibition and Conference for Power Electronics, Intelligent Motion, Renewable Energy and Energy Management, Nuremburg, Germany, 7–8 July 2020; pp. 673–680.
38. Gersem, H.D.; Muetze, A. Finite-Element Supported Transmission- Line Models for Calculating High-Frequency Effects in Machine Windings. *IEEE Trans. Magn.* **2012**, *28*, 787–791. [CrossRef]
39. Radja, N.; Rachek, M.; Larbi, S.N. Improved RLMC-Circuit HF-Dependent Parameters Using FE-EM Computation Dedicated to Predict Fast Transient Voltage Along Insulated Windings. *IEEE Trans. Electromagn. Compat.* **2019**, *61*, 301–308. [CrossRef]
40. Gersem, H.D.; Weiland, T.; Henze, O.; Binder, A. Eddy-current formulation for constructing transmission-line models for machine windings. *Eur. Phys. J. Appl. Phys.* **2010**, *49*, 1–7. [CrossRef]
41. Jorks, H.V.; Gjonaj, E.; Weiland, T.; Magdun, O.N. Three-dimensional simulations of an induction motor including eddy current effects in core laminations. *IET Sci. Meas. Technol.* **2012**, *6*, 344–349. [CrossRef]
42. Behrendt, C.N.; Dittmann, J.; Knebusch, B.; Ponick, B. Common-Mode Impedance Prediction of a High Frequency Hairpin Stator Winding Based on FEM and Modified Nodal Analysis. In Proceedings of the International Symposium on Power Electronics, Electrical Drives, Automation and Motion (SPEEDAM), Sorrento, Italy, 22–24 June 2022; pp. 20–26. [CrossRef]
43. Stockbrügger, J.O. Analytische Bestimmung Parasitärer Kapazitäten in Elektrischen Maschinen. Ph.D. Thesis, Institutionelles Repositorium der Leibniz Universitat Hannover, Hannover, Germany, 2021. [CrossRef]
44. Radnai, B.; Gemeinder, Y. *FVA 650 I: Schädlicher Stromdurchgang*; Forschungsvereinigung Antriebstechnik e.V.: Frankfurt am Main, Germany, 2015; Volume 1127.
45. Gemeinder, Y. Lagerimpedanz und Lagerschädigung bei Stromdurchgang in Umrichtergespeisten Elektrischen Maschinen. Ph.D. Thesis, Technische Universität Darmstadt, Darmstadt, Germany, 2016.
46. Hamrock, B.J.; Dowson, D. *Ball Bearing Lubrication: The Elastohydrodynamics of Elliptical Contacts*; Wiley: New York, NY, USA, 1981.
47. Schneider, V.; Liu, H.C.; Bader, N.; Furtmann, A.; Poll, G. Empirical Formulae for the Influence of Real Film Thickness Distribution on the Capacitance of an EHL Point Contact and Application to Rolling Bearings. *Tribol. Int.* **2021**, *154*, 106714. [CrossRef]
48. Bader, N.; Liu, H.; Zhang, B.B.; Poll, G. Film Thickness Measurements in EHL-Contacts Using Capacitance Measurements. In Proceedings of the Leeds-Lyon Symposium on Tribology 2019, Valpré, France, 5–10 September 2021.
49. Jablonka, K.; Glovnea, R.; Bongaerts, J. Evaluation of EHD Films by Electrical Capacitance. *J. Phys. Appl. Phys.* **2012**, *45*, 385301. [CrossRef]
50. Barz, M. Die Schmierfilmbildung in Fettgeschmierten Schnellaufenden Spindellagern. Ph.D. Thesis, Leibniz Universität Hannover, Hannover, Germany, 1996.
51. Wittek, E.; Kriese, M.; Tischmacher, H.; Gattermann, S.; Ponick, B.; Poll, G. Capacitances and Lubricant Film Thicknesses of Motor Bearings under Different Operating Conditions. In Proceedings of the 2010 XIX IEEE International Conference on Electrical Machines, Rome, Italy, 6–8 September 2010; pp. 1–6. [CrossRef]
52. Schneider, V.; Bader, N.; Liu, H.; Poll, G. Method for in Situ Film Thickness Measurement of Ball Bearings under Combined Loading Using Capacitance Measurements. *Tribol. Int.* **2022**, *171*, 107524. [CrossRef]
53. Lubrecht, A. Numerical Solution of the EHL Line and Point Contact Problem Using Multigrid Techniques. Ph.D. Thesis, University of Twente, Enschede, The Netherlands, 1987.
54. Venner, C.H. Multilevel Solution of the EHL Line and Point Contact Problems. Ph.D. Thesis, University of Twente, Enschede, The Netherlands, 1991.

55. Tischmacher, H.; Kartashov, O. Simulation von Lichtbogenentladungen in Wälzlagern von Elektromotoren zur Interpretation von experimentellen Ergebnissen an einem Lagerversuchsstand. In Proceedings of the 32. CADFEM Users' Meeting, Nürmberg, Germany, 4–6 June 2014.
56. Jagenbrein, A. Investigations of Bearing Failures Due to Electric Current Passage. Ph.D. Thesis, Technische Universität Wien, Vienna, Austria, 2005.
57. Busse, D.; Erdman, J.; Kerkman, R.; Schlegel, D.; Skibinski, G. The Effects of PWM Voltage Source Inverters on the Mechanical Performance of Rolling Bearings. *Ind. Appl. IEEE Trans.* **1997**, *33*, 567–576. [CrossRef]
58. Prashad, H. *Tribology in Electrical Environments*; Elsevier: Amsterdam, The Netherlands, 2006.
59. Zika, T. Electric Discharge Damaging in Lubricated Rolling Contacts. Ph.D. Thesis, Technische Universität Wien, Vienna, Austria, 2010.
60. Tischmacher, H.; Gattermann, S. Einflussgrößen auf Lagerströme bei umrichtergespeisten Elektromotoren. *VDI-Berichte* **2013**, *2202*, 45–59.
61. International Electrotechnical Commission. *IEC 60156: Insulating Liquids-Determination of the Breakdown Voltage at Power Frequency-Test Method*; IEC: Geneva, Switzerland, 1995.
62. Wittek, E. Charakterisierung des Schmierungszustandes im Rillenkugellager mit dem Kapazitiven Messverfahren. Ph.D. Thesis, Leibniz Universität Hannover, Hannover, Germany, 2016.
63. Skinner, J.F.; Cussler, E.L.; Fuoss, R.M. Pressure Dependence of Dielectric Constant and Density of Liquids. *J. Phys. Chem.* **1968**, *72*, 1057–1064. [CrossRef]
64. Jackson, J.D. *Classical Electrodynamics*, 3rd ed.; Wiley: New York, NY, USA, 1999.
65. Bondi, A.A. *Physical Chemistry of Lubricating Oils*; Book Division, Reinhold Pub. Corp.: New York, NY, USA, 1951.
66. Schrader, R. Die Schmierfilmbildung von Additivierten Mineralölen, synthetischen Schmierfilmflüssigkeiten und Schmierfetten im elastohydrodynamischen Wälzkontakt. Ph.D. Thesis, Leibniz Universität Hannover, Hannover, Germany, 1988.
67. Bode, B. Entwicklung eines Quarzviskosimeters fuer Messungen bei Hohen Druecken. Ph.D. Thesis, Technische Universität Clausthal, Clausthal-Zellerfeld, Germany, 1984.
68. Bode, B. Modell zur Beschreibung des Fliessverhaltens von Flüssigkeiten unter hohem Druck. *Tribol. Schmier.* **1989**, *35*, 256–261.
69. Matt, D.T.; Rauch, E. SME 4.0: The Role of Small- and Medium-Sized Enterprises in the Digital Transformation. In *Industry 4.0 for SMEs: Challenges, Opportunities and Requirements*; Matt, D.T., Modrák, V., Zsifkovits, H., Eds.; Springer International Publishing: Berlin/Heidelberg, Germany, 2020; pp. 3–36. [CrossRef]
70. Martin, G.; Vogel, S.; Schirra, T.; Vorwerk-Handing, G.; Kirchner, E. Methodical Evaluation of Sensor Positions for Condition Monitoring of Gears. In Proceedings of the DS 91: Proceedings of NordDesign, Linköping, Sweden, 14–17 August 2018.
71. Vorwerk-Handing, G.; Gwosch, T.; Schork, S.; Kirchner, E.; Matthiesen, S. Classification and Examples of next Generation Machine Elements. *Forsch. Ingenieurwesen* **2020**, *84*, 21–32. [CrossRef]
72. Lewicki, W. Some Physical Aspects of Lubrication in Rolling Bearings and Gears. Ph.D. Thesis, Birbeck College, University of London, London, UK, 1955.
73. Crook, A.W.; Allibone, T.E. The Lubrication of Rollers II. Film Thickness with Relation to Viscosity and Speed. *Philos. Trans. R. Soc. Lond. Ser. Math. Phys. Sci.* **1961**, *254*, 223–236. [CrossRef]
74. Crook, A.W. Some Physical Aspects of Lubrication and Wear. *Contemp. Phys.* **1962**, *3*, 257–271. [CrossRef]
75. Dyson, A.; Naylor, H.; Wilson, A.R. The Measurement of Oil-Film Thickness in Elastohydrodynamic Contacts. *Proc. Inst. Mech. Eng. Conf. Proc.* **1965**, *180*, 119–134. [CrossRef]
76. Bader, N.; Furtmann, A.; Tischmacher, H.; Poll, G. Capacitances and Lubricant Film Thicknesses of Grease and Oil Lubricated Bearings. In Proceedings of the STLE Annual Meeting & Exhibition, Atlanta, GA, USA, 21–25 May 2017; pp. 311–314.
77. Jablonka, K.; Glovnea, R.; Bongaerts, J. Quantitative Measurements of Film Thickness in a Radially Loaded Deep-Groove Ball Bearing. *Tribol. Int.* **2018**, *119*, 239–249. [CrossRef]
78. Schirra, T.; Martin, G.; Puchtler, S.; Kirchner, E. Electric Impedance of Rolling Bearings—Consideration of Unloaded Rolling Elements. *Tribol. Int.* **2021**, *158*. [CrossRef]
79. Schirra, T. Phänomenologische Betrachtung der sensorisch nutzbaren Effekte am Wälzlager: Einfluss unbelasteter Wälzkörper auf die elektrische Impedanz. Ph.D. Dissertation, Technische Universität Darmstadt, Darmstadt, Germany, 2020.
80. Schnabel, S.; Marklund, P.; Minami, I.; Larsson, R. Monitoring of Running-in of an EHL Contact Using Contact Impedance. *Tribol. Lett.* **2016**, *63*, 35. [CrossRef]
81. Maruyama, T.; Maeda, M.; Nakano, K. Lubrication Condition Monitoring of Practical Ball Bearings by Electrical Impedance Method. *Tribol. Online* **2019**, *14*, 327–338. [CrossRef]
82. Martin, G.; Schirra, T.; Kirchner, E. Experimental High Frequency Analysis of the Electric Impedance of Rolling Bearings. In Proceedings of the Bearing World, Würzburg, Germany, 5–6 July 2020; VDMA: Frankfurt am Main, Germany, 2020.
83. Schirra, T.; Martin, G.; Vogel, S.; Kirchner, E. Ball Bearings as Sensors for Systematical Combination of Load and Failure Monitoring. In Proceedings of the DS 92: Proceedings of the DESIGN 2018 15th International Design Conference, Dubrovnik, Croatia, 21–24 May 2018; pp. 3011–3022. [CrossRef]
84. Dahlke, H. *Handbuch Wälzlager-Technik: Bauarten, Gestaltung, Betrieb*; Springer Fachmedien: Wiesbaden, Germmany, 1994.

85. GmbH, S.M.S. (Ed.) *Condition Monitoring Praxis: Handbuch zur Schwingungs-Zustandsüberwachung von Maschinen und Anlagen*, 1st ed.; Vereinigte Fachverlage GmbH: Mainz, Germany, 2019.
86. Schiffler, A. *Steuerungsintegrierte Prozessüberwachung bei der Zerspanung mit Motorspindeln*; Schriftenreihe des PTW: "Innovation Fertigungstechnik"; Shaker: Aachen, Germany, 2011.
87. Van Hecke, B.; Yoon, J.; He, D. Low Speed Bearing Fault Diagnosis Using Acoustic Emission Sensors. *Appl. Acoust.* **2016**, *105*, 35–44. [CrossRef]
88. Renaudin, L.; Bonnardot, F.; Musy, O.; Doray, J.; Rémond, D. Natural Roller Bearing Fault Detection by Angular Measurement of True Instantaneous Angular Speed. *Mech. Syst. Signal Process.* **2010**, *24*, 1998–2011. [CrossRef]
89. Kirchner, E.; Martin, G.; Vogel, S. Sensor Integrating Machine Elements—Key to In-Situ Measurements in Mechanical Engineering. In Proceedings of the 23rd International Seminar on High Technology, Piracicaba, Brazil, 4 October 2018.
90. Martin, G. Die Wälzlagerimpedanz als Werkzeug zur Untersuchung von Oberflächenabweichungen in Wälzlagern. Ph.D. Thesis, Technische Universität Darmstadt, Darmstadt, Germany, 2021.